

Fast whole-brain imaging of seizures in zebrafish larvae by two-photon light-sheet microscopy: supplement

GIUSEPPE DE VITO,^{1,2,8}  LAPO TURRINI,^{2,3,8}  CAROLINE MÜLLENBROICH,^{2,4,5}  PIETRO RICCI,² GIUSEPPE SANCATALDO,^{2,3} GIACOMO MAZZAMUTO,^{2,5} NATASCIA TISO,⁶ LEONARDO SACCONI,^{2,5} DUCCIO FANELLI,³ LUDOVICO SILVESTRI,^{2,3,5} FRANCESCO VANZI,^{2,7} AND FRANCESCO SAVERIO PAVONE^{2,3,5,*} 

¹ University of Florence, Department of Neuroscience, Psychology, Drug Research and Child Health, Viale Pieraccini 6, Florence, Italy, 50139, Italy

² European Laboratory for Non-Linear Spectroscopy, Via Nello Carrara 1, Sesto Fiorentino 50019, Italy

³ University of Florence, Department of Physics and Astronomy, Via Sansone 1, Sesto Fiorentino 50019, Italy

⁴ School of Physics and Astronomy, Kelvin Building, University of Glasgow, G12 8QQ, Glasgow, UK

⁵ National Institute of Optics, National Research Council, Via Nello Carrara 1, Sesto Fiorentino 50019, Italy

⁶ University of Padova, Department of Biology, Via U. Bassi 58/B, Padova 35131, Italy

⁷ University of Florence, Department of Biology, Via Madonna del Piano 6, Sesto Fiorentino 50019, Italy

⁸ Co-first authors with equal contribution

*francesco.pavone@unifi.it

This supplement published with Optica Publishing Group on 16 February 2022 by The Authors under the terms of the [Creative Commons Attribution 4.0 License](https://creativecommons.org/licenses/by/4.0/) in the format provided by the authors and unedited. Further distribution of this work must maintain attribution to the author(s) and the published article's title, journal citation, and DOI.

Supplement DOI: <https://doi.org/10.6084/m9.figshare.17085794>

Parent Article DOI: <https://doi.org/10.1364/BOE.434146>

Fast whole-brain imaging of seizures in zebrafish larvae by two-photon light-sheet microscopy: supplemental document

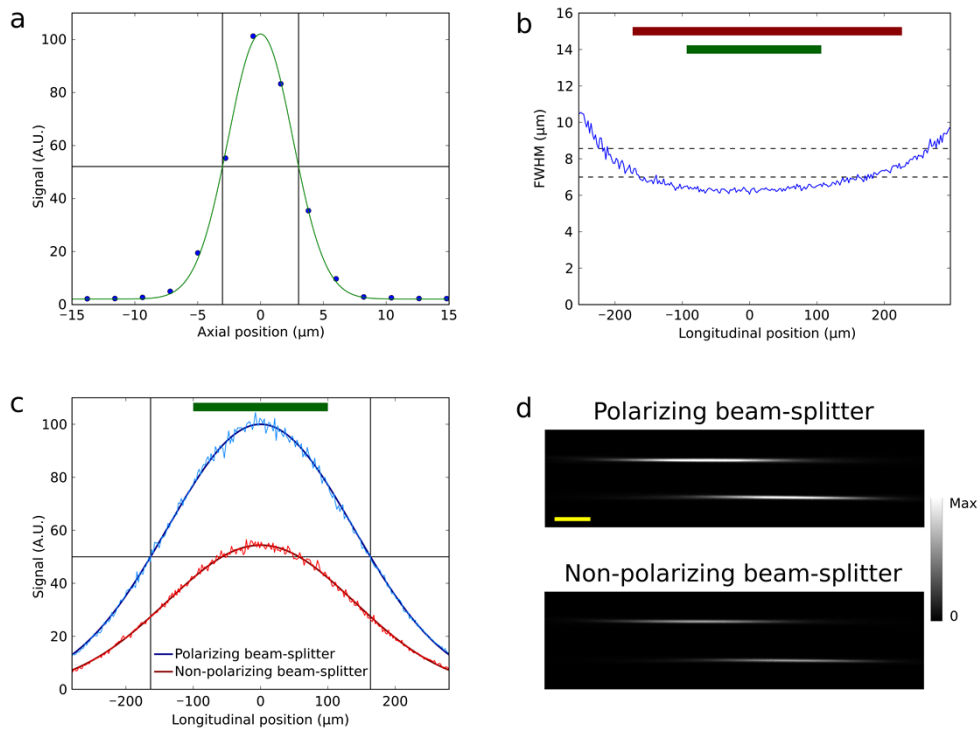


Fig. S1. (a) Transversal profile of the excitation beam at the waist. Gaussian fit in green. The single horizontal and the two vertical lines indicate the half-maximum value and the FWHM range, respectively. (b) Graph of the transversal FWHM values of the excitation beam depending on the longitudinal position along the beam. The zero value on the x-axis denotes the waist. The two dashed horizontal lines indicate the FWHM at the waist increased by a factor of $\sqrt{2}$ (8.56 μm , used to identify the confocal parameter) and the value 7 μm . The red and the green bars on the top indicate the typical size of the larval brain along the lateral dimension and half this value, respectively. (c) Longitudinal profiles of the excitation beam generated employing a polarizing (blue) or a non-polarizing (red) beam-splitter. Gaussian fitting lines (data) in darker (lighter) colors. The single horizontal and the two vertical lines indicate the half-maximum value and the FWHM range, respectively, referring to the polarizing beam-splitter condition. The green bar on the top indicates half the typical size of the larval brain along the lateral dimension. (d) Images of the two excitation beams in fluorescein solution generated employing a polarizing (top) or a non-polarizing (bottom) beam-splitter. The two beams were displaced relatively to each other along the transversal dimension purposely to improve their visualization. Scale bar: 100 μm .

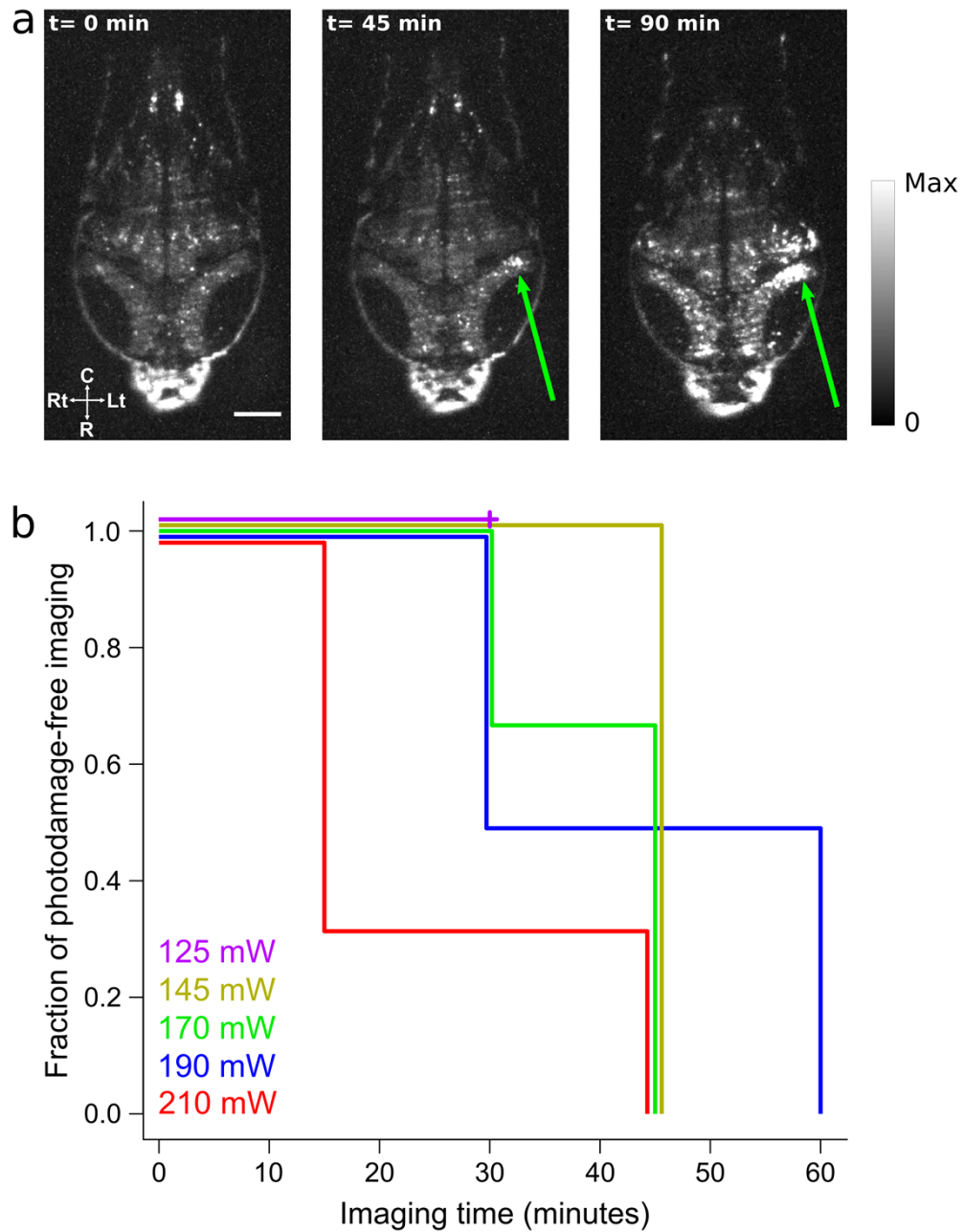


Fig. S2. (a) Coronal sections of the larval brain before the (left), at the (center) and after the (right) insurgence of the photodamage, defined as the appearance of an area of tonic neuronal calcium activity (indicated by the green arrows). The uninterrupted imaging time is reported on the panels. The images are temporal averages over 2 seconds. R: rostral, C: caudal, Rt: right, Lt: left. Scale bar: 100 μ m. (b) Survival plot depicting the fraction of larvae not showing photodamage for each time-point and tested power. Right-censoring in the 125-mW data is indicated by a cross. Adjacent lines were slightly shifted to improve visualization. Different colors indicate different cumulative excitation power levels measured at the exit of the objectives, as specified in the legend; the excitation power at the sample is estimated to be reduced by 33%. Raw data shown in Table S1.

Table S1. Cumulative illumination power at the exit of the objectives and time of appearance of photodamage for each tested larva.

Power (mW)	Time to photodamage (minutes)
125	>30
145	45
170	45
170	45
170	30
190	30
190	60
210	45
210	15
210	15

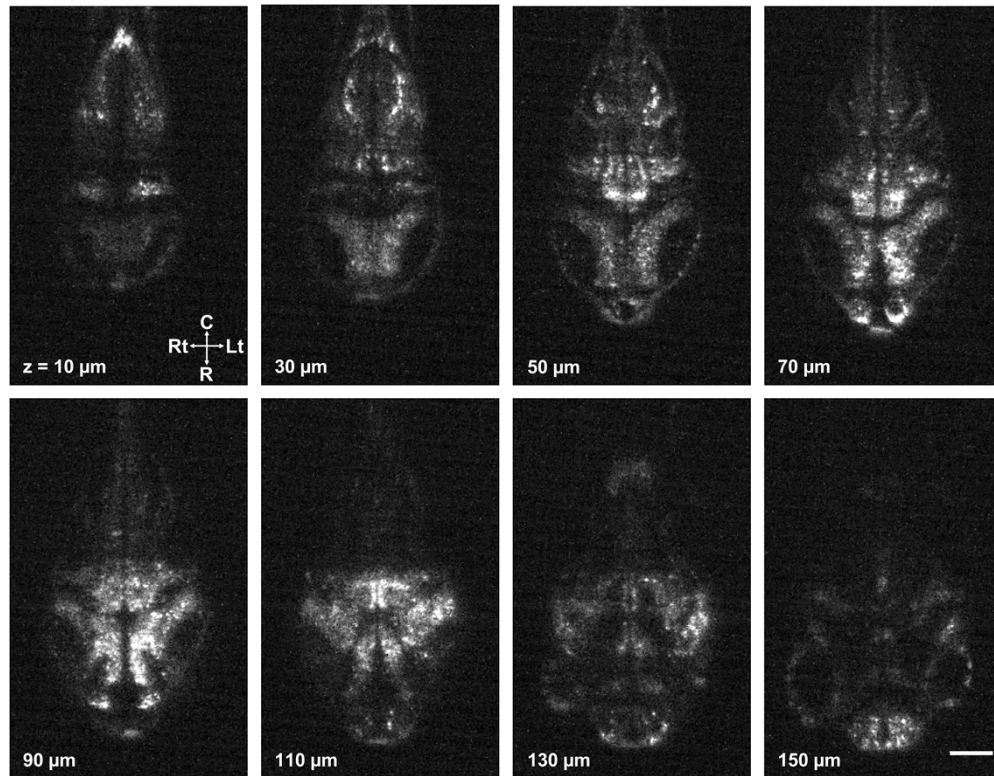


Fig. S3. Eight coronal sections showing a single temporal frame from the same time-lapse volumetric recording of Fig. 2b. The sections were recorded at different dorso-ventral depths of the larva (indicated on the panels, with respect to the dorsal surface). R: rostral, C: caudal, Rt: right, Lt: left. Scale bar: 100 μm .

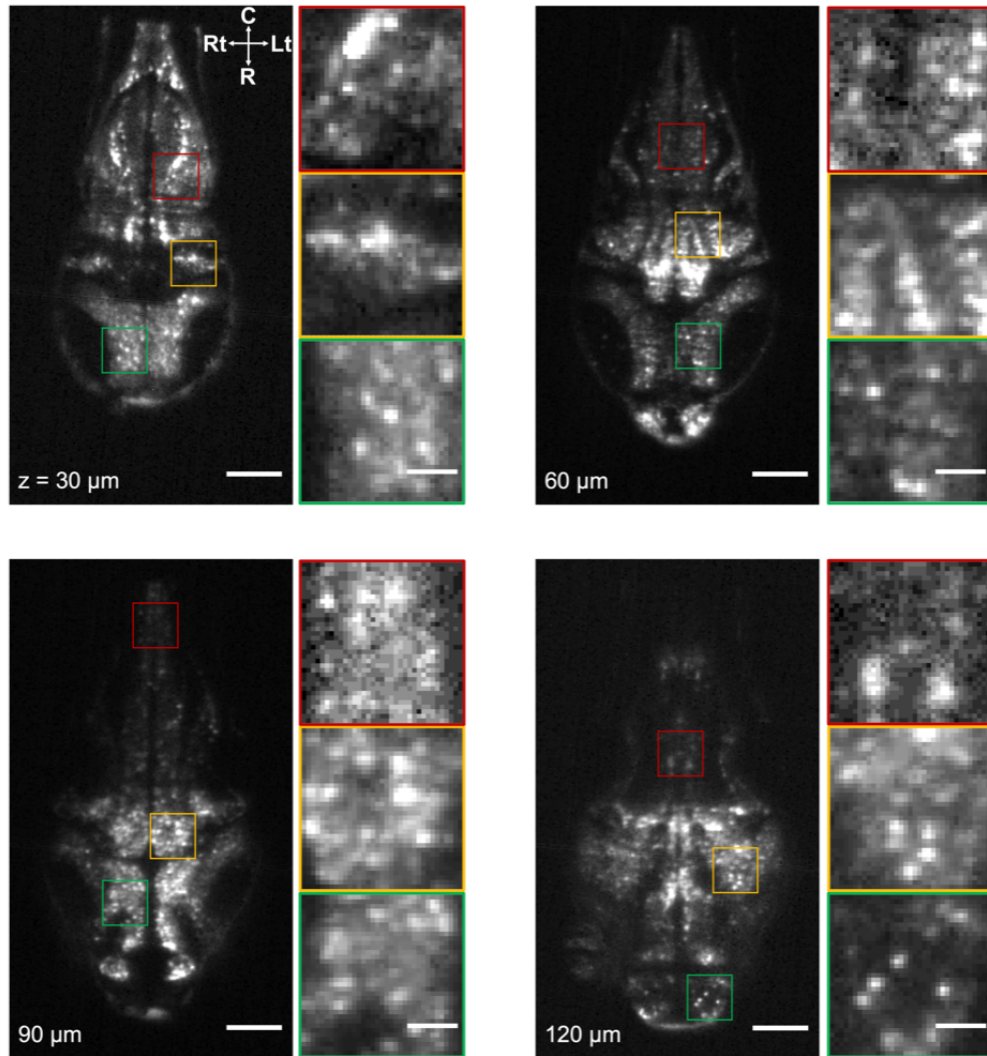


Fig. S4. Main panels: four coronal sections showing temporal average intensity projections at different dorso-ventral depths of a larval brain (indicated on the panels, with respect to the dorsal surface). R: rostral, C: caudal, Rt: right, Lt: left. Scale bar: 100 μm. Side panels: magnifications of the areas indicated by the rectangles of the same respective colors on the main panels. Brightness and contrast were optimized separately for each image to improve visibility. Scale bar: 25 μm.

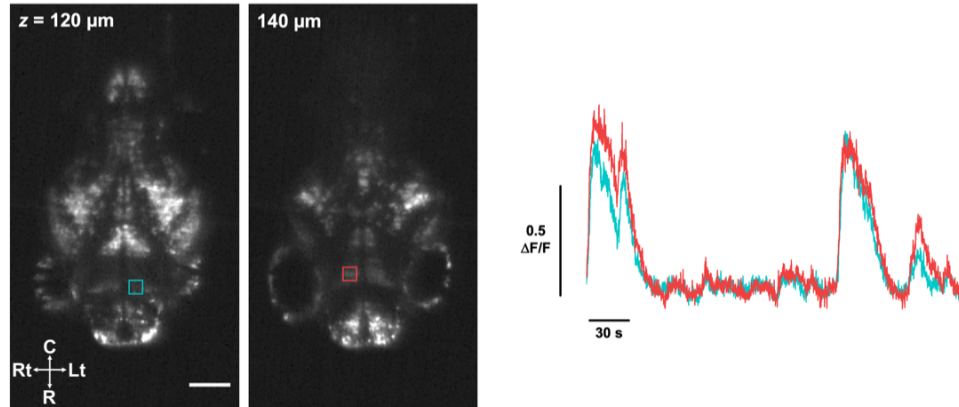


Fig. S5. Left: two coronal sections showing temporal average intensity projections at different dorso-ventral depths of a larval brain (indicated on the panels, with respect to the dorsal surface) affected by reduced image quality in the forebrain area in between the eyes. R: rostral, C: caudal, Rt: right, Lt: left. Scale bar: $100 \mu\text{m}$. Right: plot of neuronal activity over time extracted from the forebrain ROIs drawn on left panels.

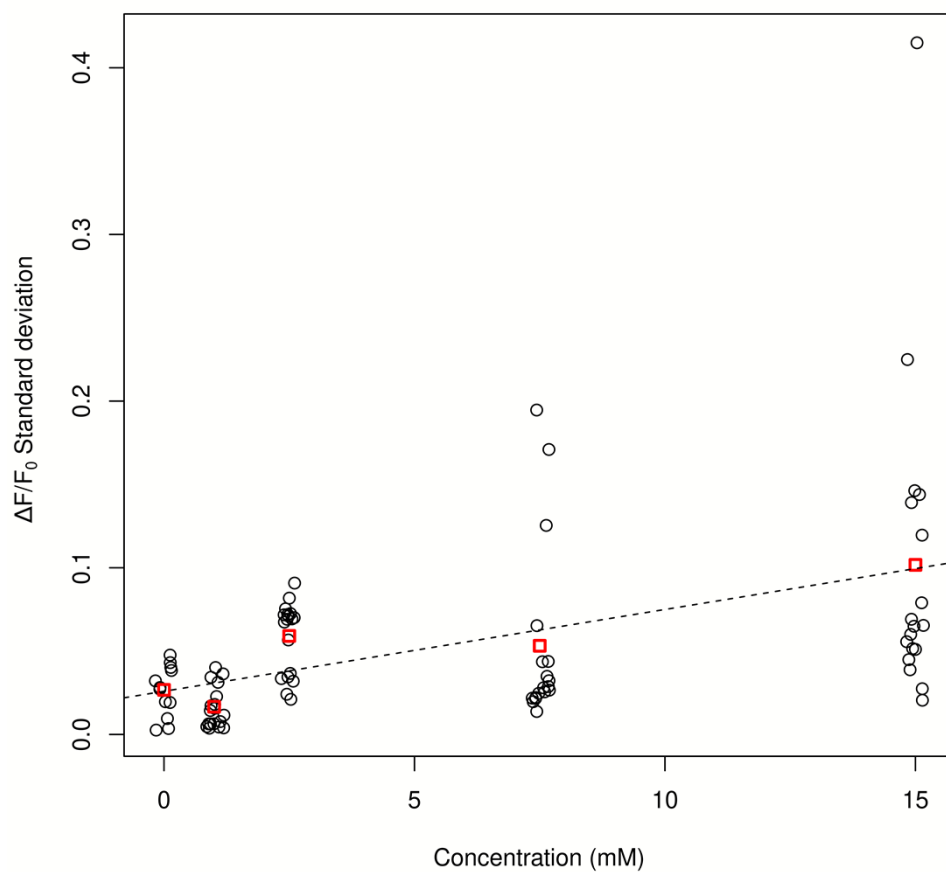


Fig. S6. Scatter plot of the standard deviation values of whole-brain-averaged $\Delta F/F_0$ traces (black hollow circles) against the PTZ concentrations. A small amount of jitter was applied on the x-axis to improve visualization. Red squares denote the average values for each PTZ concentration. The dashed line indicates the linear regression (p-value < 0.001, $R^2 \approx 0.22$).

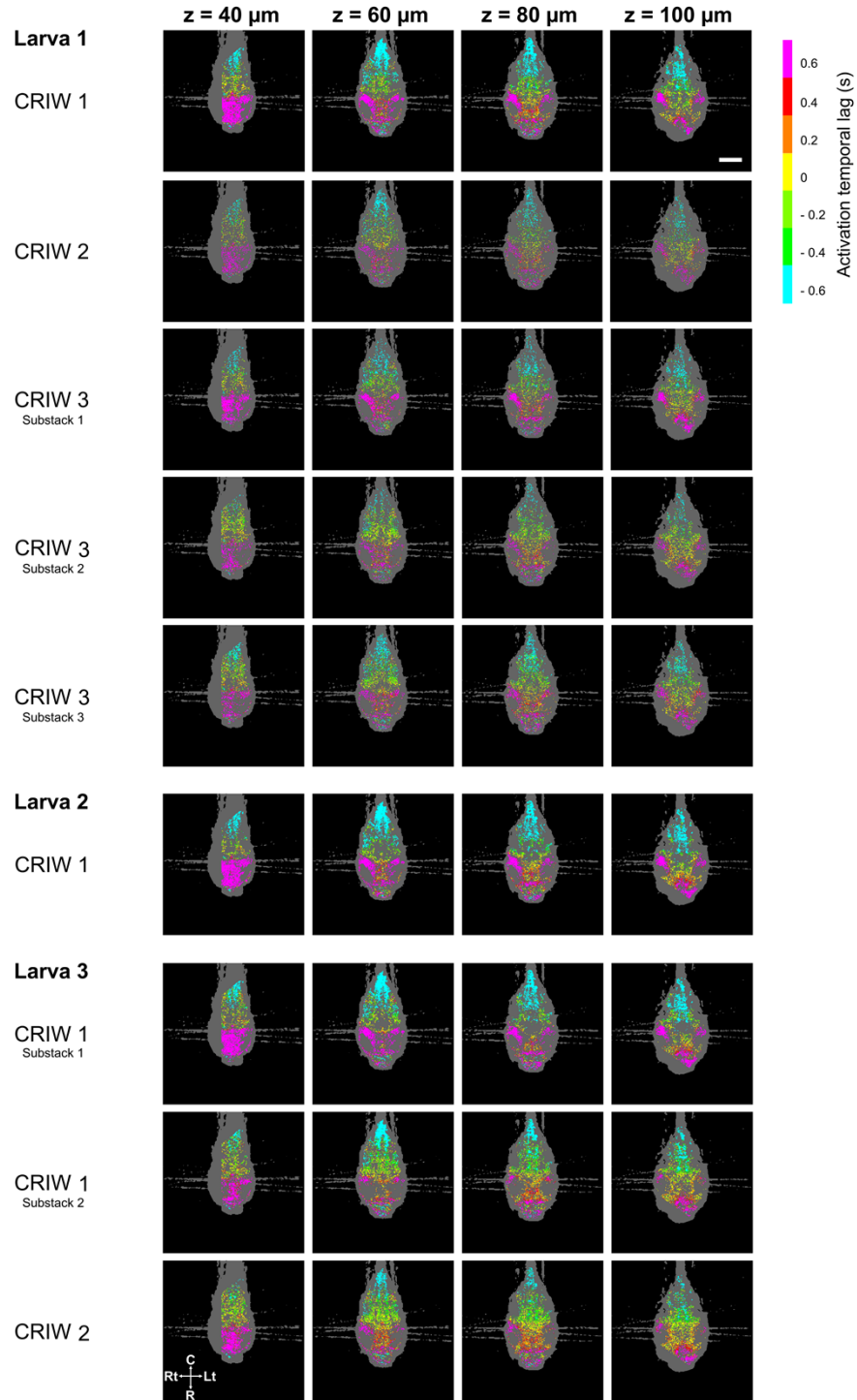


Fig. S7. These color-maps display, for each recorded CRIW event (shown along rows) from the different larvae, the voxels having the same lag-value (color) as in the aggregated color-map shown in Fig. 4c, central panel (“ICTAL”). Coronal sections at different dorso-ventral depths of a larva (indicated on the top, with respect to the dorsal surface) are shown across columns. Unmasked voxels with non-concordant lag values are displayed in grey. Color code as in Fig. 4a,c,e and as specified in the color-bar on the top-right. R: rostral, C: caudal, Rt: right, Lt: left. Scale bar: 100 μm .

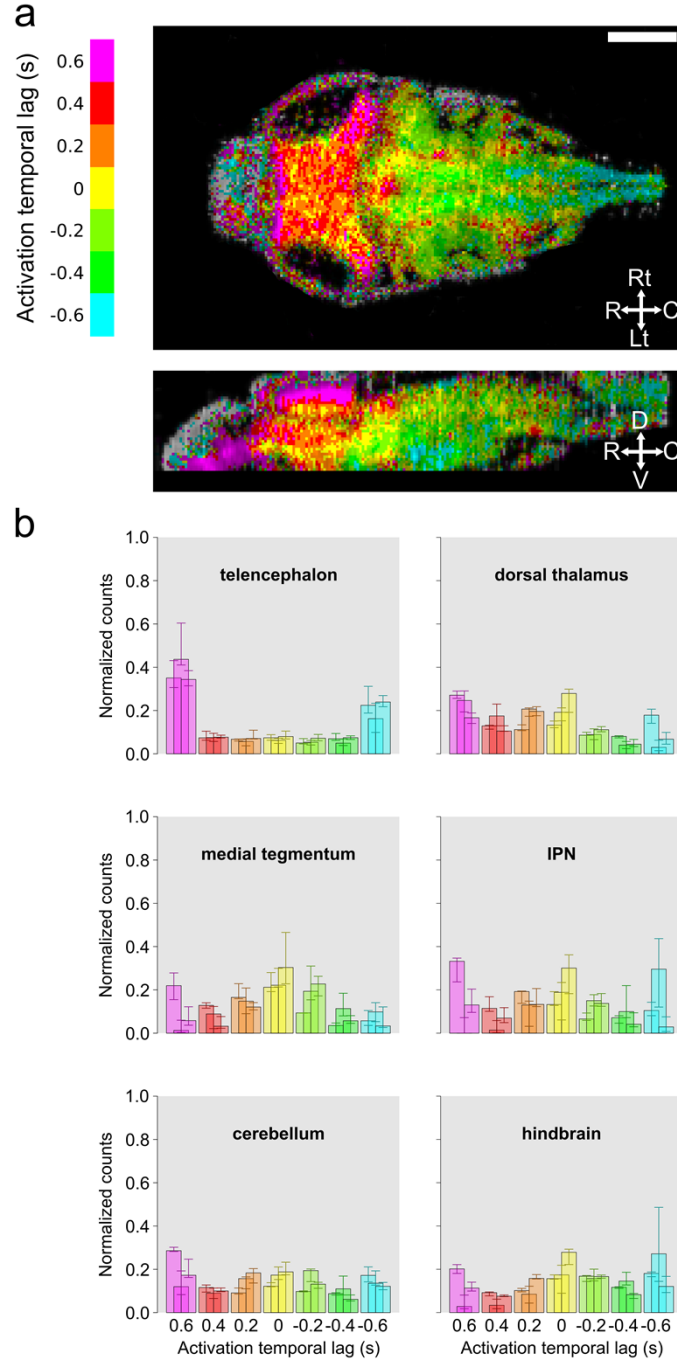


Fig. S8. (a) Lag map for a single ictal event corresponding to the calcium traces shown in Fig. 4b. Top: coronal section; bottom: sagittal section. The voxel hues encode the lag value as specified by the color map on the left and as in Fig. 4a,c,e. Masked or non-statistically significant voxels are depicted in grey values. Voxel brightness is a function of its time-averaged $\Delta F/F_0$ value. R: rostral, C: caudal, D: dorsal, V: ventral, Rt: right, Lt: left. Scale bar: 100 μm . (b) Bar plots showing the relative frequencies of the voxel-based lag values for each ROI not shown in Fig. 4e (as indicated on the plots). The bar colors correspond to the color code used in (a). The height of each bar corresponds to the median value of the single-acquisition-based frequency distribution, while the error bars indicate the first and the third quartiles of the distribution. The first, second and third bars in each lag class correspond to the control, ictal and postictal situations, respectively.

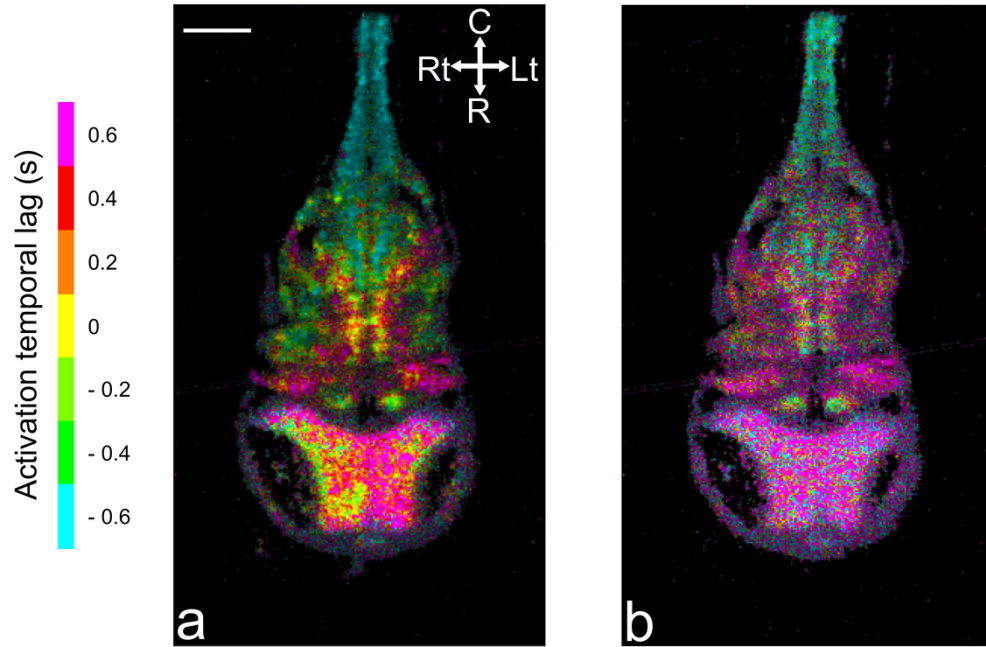


Fig. S9. Lag maps (coronal sections) for a single ictal event. (a) Results obtained with the cross-correlation based method (described in section “2.8 Voxel-based lag analysis”). R: rostral, C: caudal, Rt: right, Lt: left. (b) Results obtained with the time-derivative-method described in [54]. The voxel hues encode the lag value as specified by the color map on the left and as in Fig. 4a,c,e. The voxel saturation is kept at maximum. Scale bar: 100 μ m.

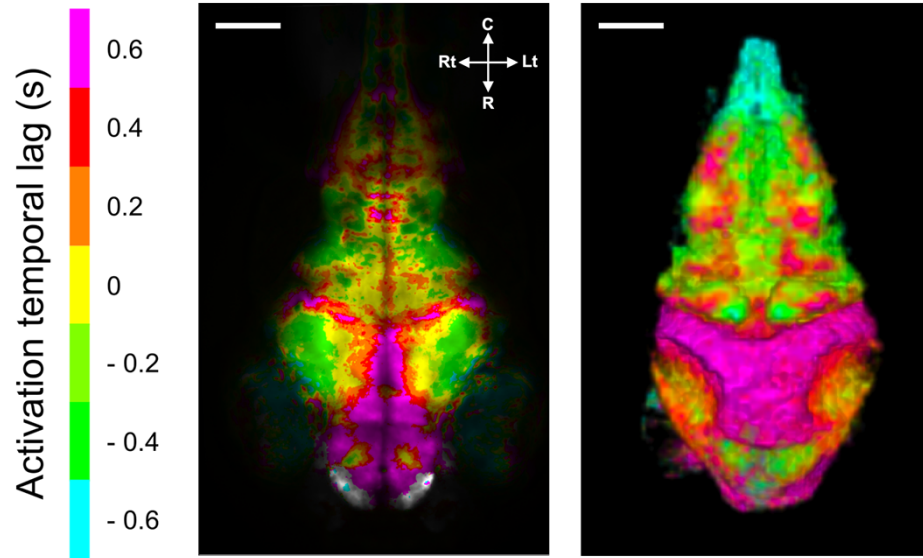


Fig. S10. Median lag map of three ictal events recorded using 1P wide-field fluorescence microscopy in a 4-dpf Tg(elavl3:GCaMP6s) zebrafish larva treated with 15 mM PTZ (left) and dorsal view of the lag map during ictal activity presented in Fig. 4a (right). The voxel hues encode the lag value as specified by the color map on the left and as in Fig. 4a,c,e. Non-statistically significant voxels are depicted in grey values. R: rostral, C: caudal, Rt: right, Lt: left. Scale bar: 100 μ m.

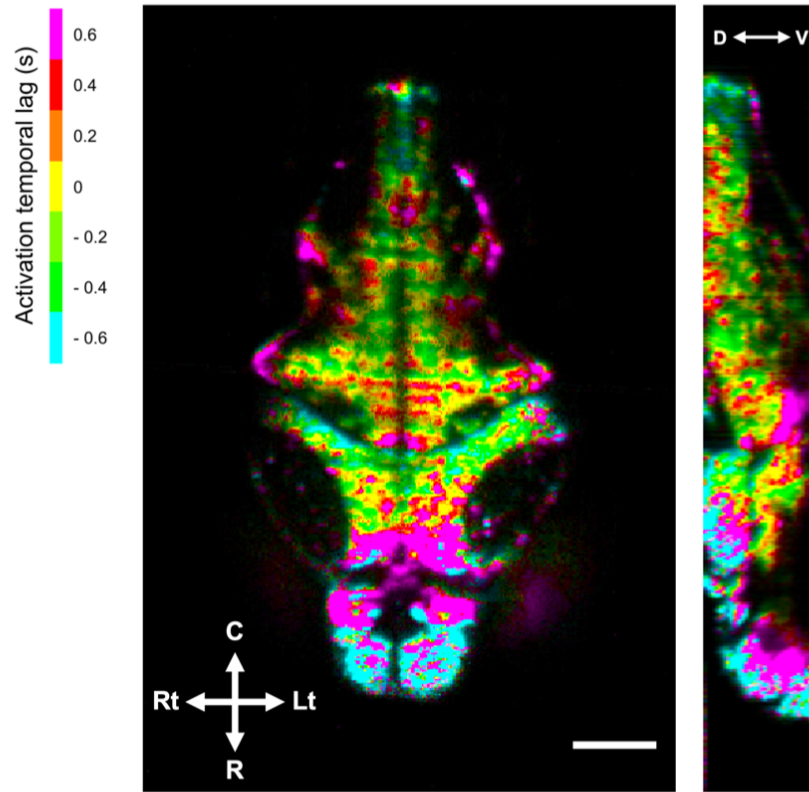


Fig. S11. Median lag map (left: coronal section; right: sagittal section) of 6 ictal events recorded in 6 dpf Tg(H2B-GCaMP6s) larvae exposed to 10 mM PTZ, as in Ref. [54]. The voxel hues encode the lag value as specified by the color map on the left and as in Fig. 4a,c,e. R: rostral, C: caudal, D: dorsal, V: ventral, Rt: right, Lt: left. Scale bar: 100 μ m.